

Large-scale cross-modality pretrained model enhances cardiovascular state estimation and cardiomyopathy detection from electrocardiograms: An AI system development and multi-center validation study

Zhengyao Ding^{1*}, Yujian Hu^{2*}, Youyao Xu⁵, Chengchen Zhao⁶, Ziyu Li¹, Yiheng Mao¹, Haitao Li¹, Qian Li,⁴ Jing Wang³, Yue Chen³, Mengjia Chen³, Longbo Wang³, Xuesen Chu⁷, Weichao Pan⁸, Ziyi Liu⁸, Fei Wu^{1,#}, Hongkun Zhang^{2,#}, Ting Chen^{3,#}, Zhengxing Huang^{1,#}

¹ College of Computer Science and Technology, Zhejiang University, Hangzhou, China

² Department of Vascular Surgery, The First Affiliated Hospital of Zhejiang University School of Medicine, Hangzhou, China

³ Department of Cardiology, The First Affiliated Hospital, Zhejiang University School of Medicine, Hangzhou, Zhejiang Province, China

⁴ Department of Radiology, The First Affiliated Hospital, Zhejiang University School of Medicine, Hangzhou, Zhejiang Province, China

⁵ Department of Vascular Surgery, Quzhou People's Hospital, Quzhou, China

⁶ Department of Cardiology, The Second Affiliated Hospital of Zhejiang University School of Medicine, Hangzhou, China

⁷ China Ship Scientific Research Center, Wuxi, China

⁸ Guangdong Transtek Medical Electronics Co., Ltd., Zhongshan, China

Corresponding authors

* These authors contributed equally to this work.

Abstract

Cardiovascular diseases (CVDs) present significant challenges for early and accurate diagnosis. While cardiac magnetic resonance imaging (CMR) is the gold standard for assessing cardiac function and diagnosing CVDs, its high cost and technical complexity limit accessibility. In contrast, electrocardiography (ECG) offers promise for large-scale early screening. This study introduces CardiacNets, an innovative model that enhances ECG analysis by leveraging the diagnostic strengths of CMR through cross-modal contrastive learning and generative pretraining. CardiacNets serves two primary functions: (1) it evaluates detailed cardiac function indicators and screens for potential CVDs, including coronary artery disease, cardiomyopathy, pericarditis, heart failure and pulmonary hypertension, using ECG input; and (2) it enhances interpretability by generating high-quality CMR images from ECG data. We train and validate the proposed CardiacNets on two large-scale public datasets (the UK Biobank with 41,519 individuals and the MIMIC-IV-ECG comprising 501,172 samples) as well as three private datasets (FAHZU with 410 individuals, SAHZU with 464 individuals, and QPH with 338 individuals), and the findings demonstrate that CardiacNets consistently outperforms traditional ECG-only models, substantially improving screening accuracy. Furthermore, the generated CMR images provide valuable diagnostic support for physicians of all experience levels. This proof-of-concept study highlights how ECG can facilitate cross-modal insights into cardiac function assessment, paving the way for enhanced CVD screening and diagnosis at a population level.

Main

Cardiovascular diseases (CVDs) remain the leading cause of mortality worldwide, with their share of global deaths increasing significantly in recent years¹⁻³. Notably, the mortality rate associated with cardiomyopathy has risen by 7.6% during this period, contributing to an escalating burden of disease⁴. The multifaceted nature of CVD presentations often results in missed or misdiagnosed cases in clinical practice, leading to delays in treatment and inadequate patient care^{5,6}. To effectively assess cardiovascular health, clinicians utilize a variety of diagnostic modalities, including electrocardiography (ECG)⁷ and cardiovascular magnetic resonance imaging (CMR)⁸. ECG measures the electrical potential differences within the heart and is widely employed to detect cardiac abnormalities such as myocardial infarction and arrhythmias. Its non-invasive and cost-effective nature has facilitated its adoption across healthcare institutions, making it accessible at all levels⁹. In contrast, CMR is a comprehensive imaging modality that excels in evaluating cardiac morphology, function, myocardial perfusion, and tissue characterization, providing a more detailed assessment of cardiac status¹⁰⁻¹³. As such, CMR is regarded a common and effective diagnostic tool for CVDs¹⁴, particularly structural heart conditions like cardiomyopathy¹⁵⁻¹⁷. However, the high costs and operational complexities associated with CMR limit its accessibility¹⁸, especially in developing countries and rural areas. Given this context, there is an urgent need to explore methodologies that can leverage ECG as a viable alternative to CMR for assessing cardiac health and conducting preliminary screenings for cardiovascular diseases. By harnessing the advantages of ECG, we can potentially enhance diagnostic capabilities and improve patient outcomes in settings where advanced imaging techniques are not readily available.

In response to urgent clinical need, the recent emergence of large-scale multimodal datasets, such as the UK Biobank (UKB) and MIMIC^{19,20}, combined with rapid advancements in deep learning technologies, presents a transformative opportunity to address existing challenges in healthcare. Cross-modal contrastive learning approaches, exemplified by CLIP (Contrastive Language-Image Pre-training)²¹, have demonstrated remarkable potential in aligning latent representations from diverse modalities through the creation of a shared embedding space. This innovative capability enables high-precision tasks, including zero-shot classification, which empowers models to make accurate predictions without the necessity for task-specific training. Moreover, generative models like Stable Diffusion model²² leverage the text encoder from CLIP as a conditional guide, facilitating the generation of highly realistic images that closely correspond to textual descriptions. These advancements underscore the power of cross-modal relationships in enhancing the capabilities of individual modalities and advancing artificial intelligence systems in healthcare. By integrating these cutting-edge technologies, researchers can develop more effective disease screening and diagnostic tools, as well as novel treatment strategies, ultimately improving patient outcomes and transforming the landscape of clinical practice.

Building on the foundation of cross-modal approaches and previous studies²³⁻²⁵, we propose a novel approach for cross-modal alignment and generative pretraining, named CardiacNets. Unlike traditional methods that focus on aligning text-image pairs with similar informational content²¹, our model emphasizes the relationship between a robust modality—one that conveys rich, comprehensive information—and a weaker modality, aiming to enhance the latter's capabilities through insights gained from the former. While earlier approaches have jointly analyzed ECG and CMR data²³, CardiacNets is specifically tailored for cardiac disease screening, demonstrating significant improvements in both diagnostic performance and the quality of CMR generation. The proposed solution consists of two primary components. First, we implement contrastive learning to align ECG data with their

corresponding CMR images, enabling a more nuanced understanding of cardiac conditions. By leveraging the strengths of each modality, CardiacNets aims to not only improve the accuracy of CVD screening, but also enhance the generation of clinically relevant images, ultimately contributing to more effective patient care. Second, the ECG encoder, trained through contrastive learning, is subsequently frozen and employed as a conditional encoder within a diffusion model. This aligned ECG representation effectively guides a latent video diffusion model²⁶—a state-of-the-art approach in the realm of computer-generated video—in producing high-quality CMR sequences that correspond to the ECG inputs. The generated CMR sequences significantly enhance the interpretability of ECG-based predictions, offering clinicians a more profound understanding of their patients' cardiovascular status.

This study aims to develop and validate a deep learning solution that utilizes ECG as a surrogate for CMR in assessing cardiac status and downstream CVD screening. Our approach is structured into two phases, as illustrated in Fig.1: (1) cross-modal contrastive learning utilizing ECG and CMR data and ECG-based CMR Image Generation Model, (2) comprehensive evaluation of downstream tasks. In the first phase, cross-modal pre-training enables ECG to capture corresponding CMR information and generate CMR images. The second phase demonstrates the superiority of the cross-modal pretrained ECG model over traditional single-modality supervised learning models that rely solely on ECG data across all evaluated downstream tasks. Notably, we observed a remarkable 21.4% improvement in cardiac indicators assessment using the UK Biobank dataset and an 8.7% enhancement in pericarditis screening on the MIMIC dataset. In several downstream tasks, the performance of the pretrained model approached that of CMR-based supervised learning models. Moreover, high-fidelity CMR images generated by the diffusion model, highlight the capabilities of our proposed model in visualization and interpretability. Finally, a reader study revealed that our model significantly enhances clinicians' ability to screen for cardiomyopathy, showcasing its practical utility in real-world clinical settings.

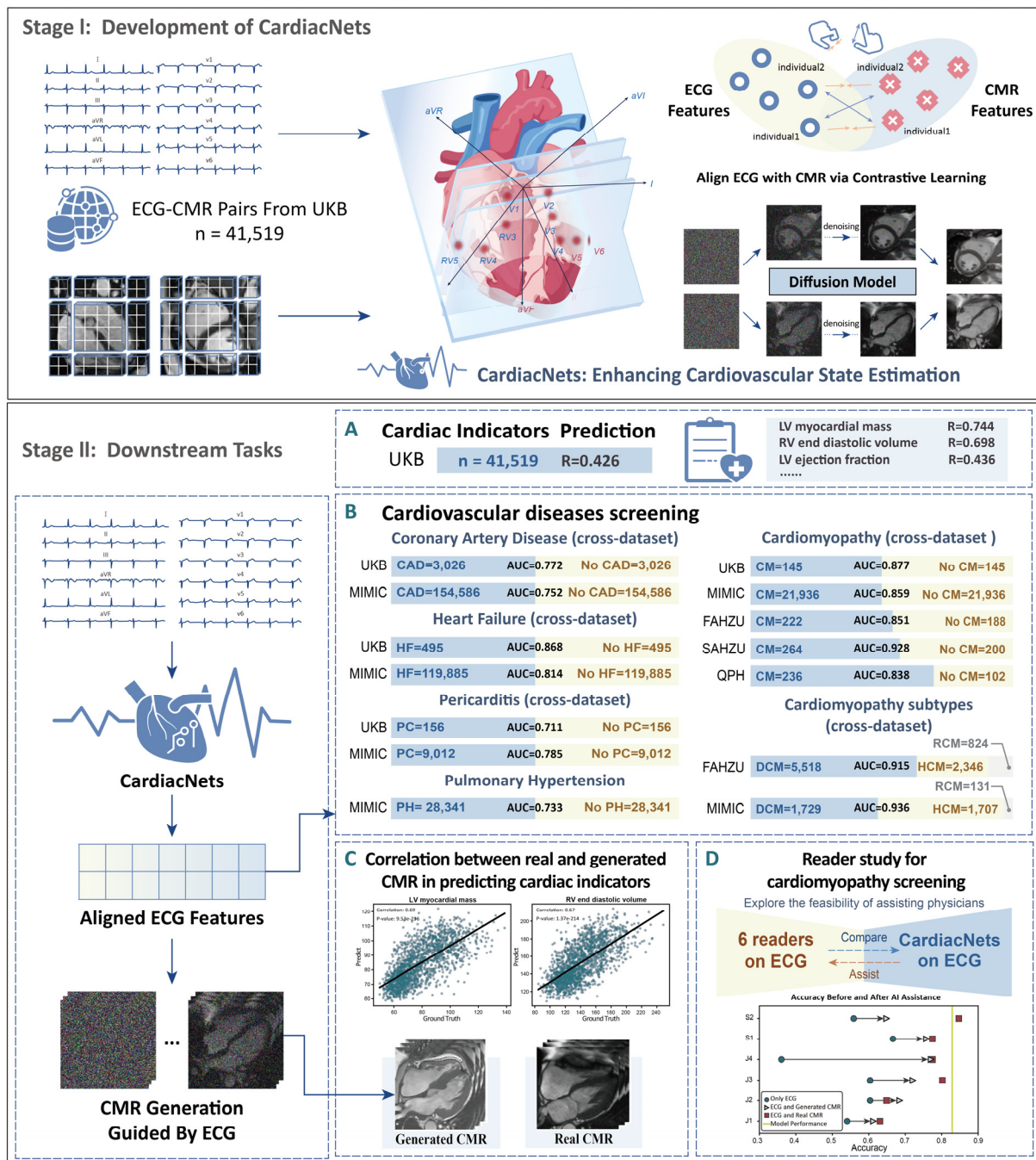


Fig. 1: Overview of the study design. **Stage I:** Development of CardiacNets. Using the UKB dataset, we trained two core components of CardiacNets: (1) an ECG model trained with ECG-CMR contrastive learning to capture relevant information from CMR, and (2) a CMR generation model trained with a video diffusion model conditioned on ECG. **Stage II:** Downstream tasks. The datasets used are from UKB, MIMIC-IV-ECG, The First Affiliated Hospital of Zhejiang University School of Medicine (FAHZU), The Second Affiliated Hospital of Zhejiang University School of Medicine (SAHZU), Quzhou People's Hospital (QPH). All tasks used only ECG data to validate the model's performance, including: (A) Prediction of cardiac indices, (B) Screening for cardiovascular diseases, particularly cardiomyopathy, (C) Correlation analysis between generated and real CMR in predicting cardiac indices, and (D) Reader study for cardiomyopathy screening.

Results

Screening for Cardiovascular diseases and cardiac phenotype prediction

We utilized two public datasets (UKB and MIMIC) and three private datasets (FAHZU, SAHZU, and QPH) to evaluate the performance of the fine-tuned model in predicting cardiac structural phenotypes and various CVD conditions (Fig. 2). In the UKB dataset (Fig. 2a), which includes paired CMR images, we compared the performance of CardiacNets against standalone ECG-based supervised learning and standalone CMR-based supervised learning. Across all diseases, CardiacNets demonstrated significant improvement over the ECG-only models ($p < 0.05$), particularly in cardiomyopathy, achieving an AUC of 87.65% compared to 72.56% for the ECG-only model. Furthermore, when comparing CardiacNets with CMR-based supervised learning, no significant difference was observed for most diseases ($p > 0.05$), except for CAD. This suggests that CardiacNets can nearly match the performance of CMR-based models in most cases.

For cardiac phenotype prediction, we incorporated 82 cardiac phenotypes published by the UKB, including left and right atrial ejection fractions and end-diastolic/systolic volumes for both atria. These indicators provide valuable insights into the detailed structure and overall state of the heart. The average Pearson correlation coefficients for these 82 indicators were as follows: CardiacNets achieved an average of 0.426, while ECG-based and CMR-based models had averages of 0.351 and 0.612, respectively. Regression plots for each indicator can be found in Supplementary Fig. 1. Although CardiacNets demonstrated significant improvement over the ECG-only model, there remains a notable gap compared to the CMR-based model. In the MIMIC dataset (Fig. 2b), where paired CMR data was unavailable, we compared CardiacNets with the ECG-only supervised learning model. As in the UKB dataset, CardiacNets significantly outperformed the ECG-only model ($p < 0.0001$).

We also validated the model's performance on three private datasets for cardiomyopathy. Using models trained on the MIMIC dataset (including both ECG-CMR pre-trained models and those trained solely on ECG), we applied them directly to the three private datasets to assess generalization. The results consistently showed that the pre-trained models outperformed the ECG-only models, with significant differences observed in the FAHZU dataset ($p < 0.0001$), SAHZU dataset ($p < 0.01$), and QPH dataset ($p < 0.05$). Moreover, the results across all three private datasets were comparable to or exceeded those from the MIMIC dataset, further emphasizing the robustness and generalizability of the models. These findings highlight the efficiency and effectiveness of CardiacNets across a wide range of settings. Additional quantitative results can be found in Supplementary Tables 1-3.

Label efficiency for disease screening

Label efficiency refers to the amount of training data and labels required to achieve a target performance level for a specific downstream task, highlighting the annotation workload for medical experts. CardiacNets demonstrated remarkable label efficiency across various disease screening tasks in the MIMIC dataset (Fig. 2c). Notably, CardiacNets outperformed standalone ECG-based models while using only 10% of the training data, underscoring the potential to address data scarcity. This capability is crucial for real-world applications, as it alleviates the annotation burden on clinical experts, making the model more applicable across diverse healthcare settings.

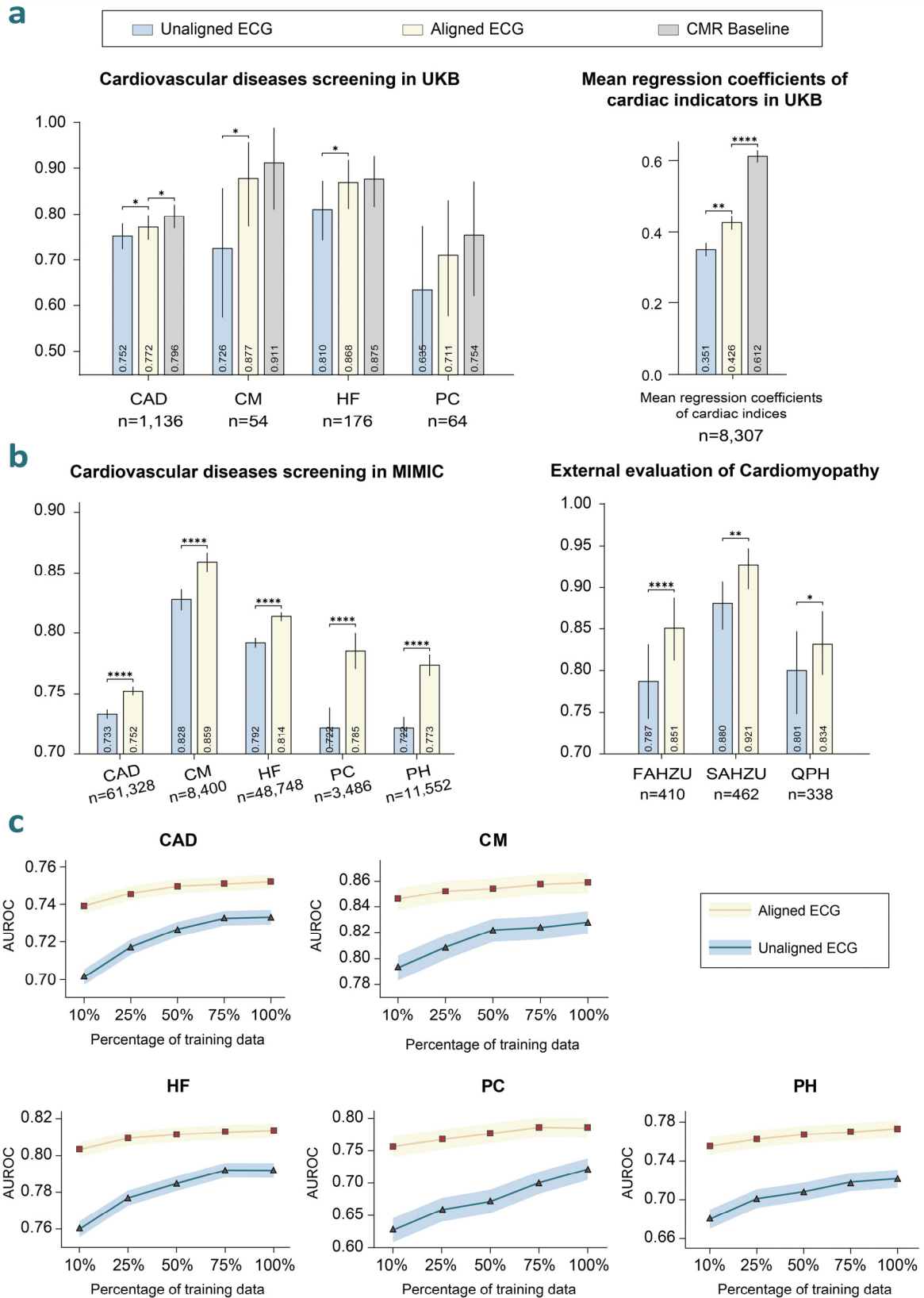


Fig. 2: Overall assessment of cardiovascular status and label utilization efficiency. a. The classification AUC metrics for coronary artery disease (CAD), cardiomyopathy (CM), pericarditis (PC), and heart failure (HF), along with the average R values for cardiac structural indicators (detailed results can be found in

Supplementary Fig. 1), were assessed in the UKB dataset. We evaluated the performance of CardiacNets against models trained with unaligned ECG data and those using CMR for supervised learning. **b.** Screening of CVDs, including CAD, CM, PC, HF, and pulmonary hypertension (PH), in the MIMIC dataset, and external validation for cardiomyopathy screening. Due to the absence of corresponding CMR images in the MIMIC dataset, we compared CardiacNets with unaligned ECG models. In both **panels a and b**, statistical significance was assessed using two-sided z-tests ($*p < 0.05$, $**p < 0.01$, $***p < 0.001$, $****p < 0.0001$). **c.** Label efficiency was analyzed by measuring the model’s performance with varying fractions of training data, providing insight into the amount of data required to achieve target performance levels.

Additionally, CardiacNets demonstrated consistently high adaptation efficiency (Extended Fig. 1), indicating that the model required less time to adjust to downstream tasks. For example, CardiacNets could reduce training time by approximately 80% to achieve convergence in predicting cardiomyopathy. This substantial reduction in training time significantly lowers computational costs, especially when utilizing effective techniques like early stopping.

Screening for subtypes of cardiomyopathy

To evaluate our model’s ability to enhance cardiomyopathy screening, we validated its performance on both the MIMIC and FAHZU datasets. In the MIMIC dataset, CardiacNets demonstrated significant improvements over the ECG-only model (Fig. 3a), with AUC scores increasing from 0.762 to 0.907 for restrictive cardiomyopathy, from 0.767 to 0.950 for dilated cardiomyopathy, and from 0.741 to 0.951 for hypertrophic cardiomyopathy. The confusion matrix for the three-class classification indicated that using unaligned ECG data resulted in an accuracy of 67.0% and an average accuracy of 52.1%. In contrast, employing pre-trained aligned ECG data improved accuracy to 86.6% and average accuracy to 73.5%.

Similarly, CardiacNets performed exceptionally well on the FAHZU dataset (Fig. 3b), achieving an average improvement of 20% across all subtypes. The confusion matrix revealed that unaligned ECG data yielded an accuracy of 66.3% and an average accuracy of 49.7%, while pre-trained ECG data achieved an accuracy of 77.8% and an average accuracy of 76.3%, indicating a substantial enhancement.

Analysis of the confusion matrices from both datasets showed that the most significant improvement was observed in restrictive cardiomyopathy, highlighting the model’s effectiveness in low-sample environments (Supplementary Tables 4-5). Collectively, these findings demonstrate that our AI model provides more nuanced subtype screening for cardiomyopathy, exhibiting strong generalizability across datasets from diverse sources.

Evaluation of CMR generation and Interpretation studies

In our CardiacNets model, ECG signals are transformed into CMR images using a video diffusion model, where the ECG serves as a conditioning input to guide the generation of these images. As illustrated in Fig. 4a, the ECG-to-CMR transformation effectively captures key phenotypes derived from CMR, such as left ventricular mass (LVM) and right ventricular end-diastolic volume (RVEDV).

To visualize the corresponding ECG signals, we used gradient-weighted class activation mapping (Grad-CAM) ²³ to generate heatmaps. A comparison of cases reveals that pre-trained aligned ECGs highlight

more regions than unaligned ECGs, demonstrating that alignment enables the model to capture a broader range of ECG details, which enhances its performance in downstream tasks—something that standalone ECGs cannot achieve. Additionally, we generated CMR images to illustrate distinct presentations in cases with various cardiovascular conditions, accompanied by the corresponding ECG heatmaps (Supplementary Table. 8).

To qualitatively assess CardiacNets' ability to generate CMR images, we also conducted a quantitative analysis. Following the methodology of Adityanarayanan et al²³, we performed a correlation analysis between the cardiac phenotypes predicted from the generated CMRs and those obtained from real CMRs. The results, illustrated in Fig. 4b-c, confirm that the LVM and RVEDV values predicted from the generated CMRs positively correlate with those from actual CMRs, demonstrating that our results surpass those reported by Adityanarayanan et al²³. For additional correlation analysis plots of other indicators, please refer to Supplementary Fig. 2. Moreover, the generated CMR images exhibit significantly higher clarity. These findings indicate that CardiacNets can effectively generate CMR images conditioned on ECG signals, successfully capturing relevant CMR-derived phenotypes and disease-specific information.

Reader Study

To further assess the performance of our AI model in a real-world clinical setting, we conducted a reader study using a new independent testing set comprising 111 subjects (77 patients with cardiomyopathy and 34 without) who were consecutively admitted to The First Affiliated Hospital of Zhejiang University School of Medicine in 2024. This testing set was carefully designed to be unselected, ensuring that it accurately reflects the true clinical prevalence.

The study was conducted in two stages. In the first stage, physicians with varying levels of experience in CMR interpretation independently assessed each patient for cardiomyopathy based solely on ECG signals. The reader cohort consisted of four junior physicians with 3–5 years of experience and two senior physicians with over 10 years of experience. After a washout period of at least one month, the second stage took place, during which the readers were provided with both real and AI-generated long- and short-axis CMR images and re-evaluated each patient.

As illustrated in Fig. 5a-b, most physicians struggled to perform effectively when relying solely on ECG signals for cardiomyopathy screening. However, their performance markedly improved with the aid of AI-generated images, with some achieving accuracy levels comparable to those observed when analyzing actual CMR data. Notably, when assessing real CMRs, most physicians underperformed compared to the model (AUC 86.5%). Although one senior physician matched the model's performance when analyzing real CMRs, it is crucial to highlight that the model based all its predictions solely on ECG input. More comprehensive experimental results are available in Supplementary Table. 9.

Additionally, we conducted a consistency analysis to assess the agreement between physicians' evaluations based on real and AI-generated CMRs, defined as the percentage of identical assessments out of the total cases (Fig. 5c). The average consistency rate among junior physicians was 71%, while senior physicians exhibited a lower rate of 58.5%, likely due to their more nuanced evaluations.

We also highlighted three cases (Fig. 5d) in which patients were initially missed during ECG reviews

but were correctly identified as having cardiomyopathy with the assistance of AI. Full ECG and CMR images are available in the supplementary materials. These findings suggest that the CMR images generated by CardiacNets can effectively capture critical information present in real CMRs, demonstrating the potential to aid physicians in screening for cardiomyopathy using only ECG data in real clinical scenarios.

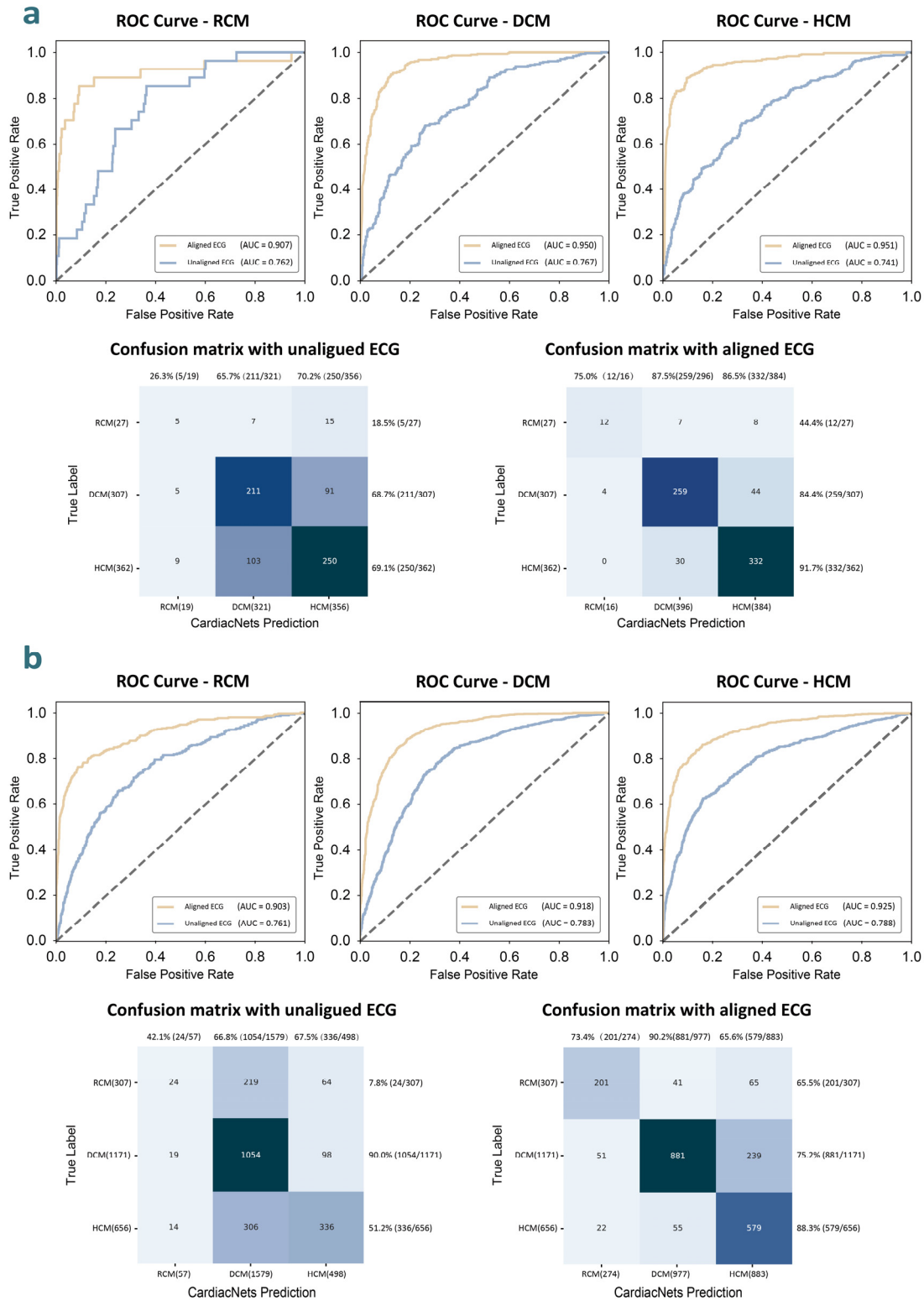
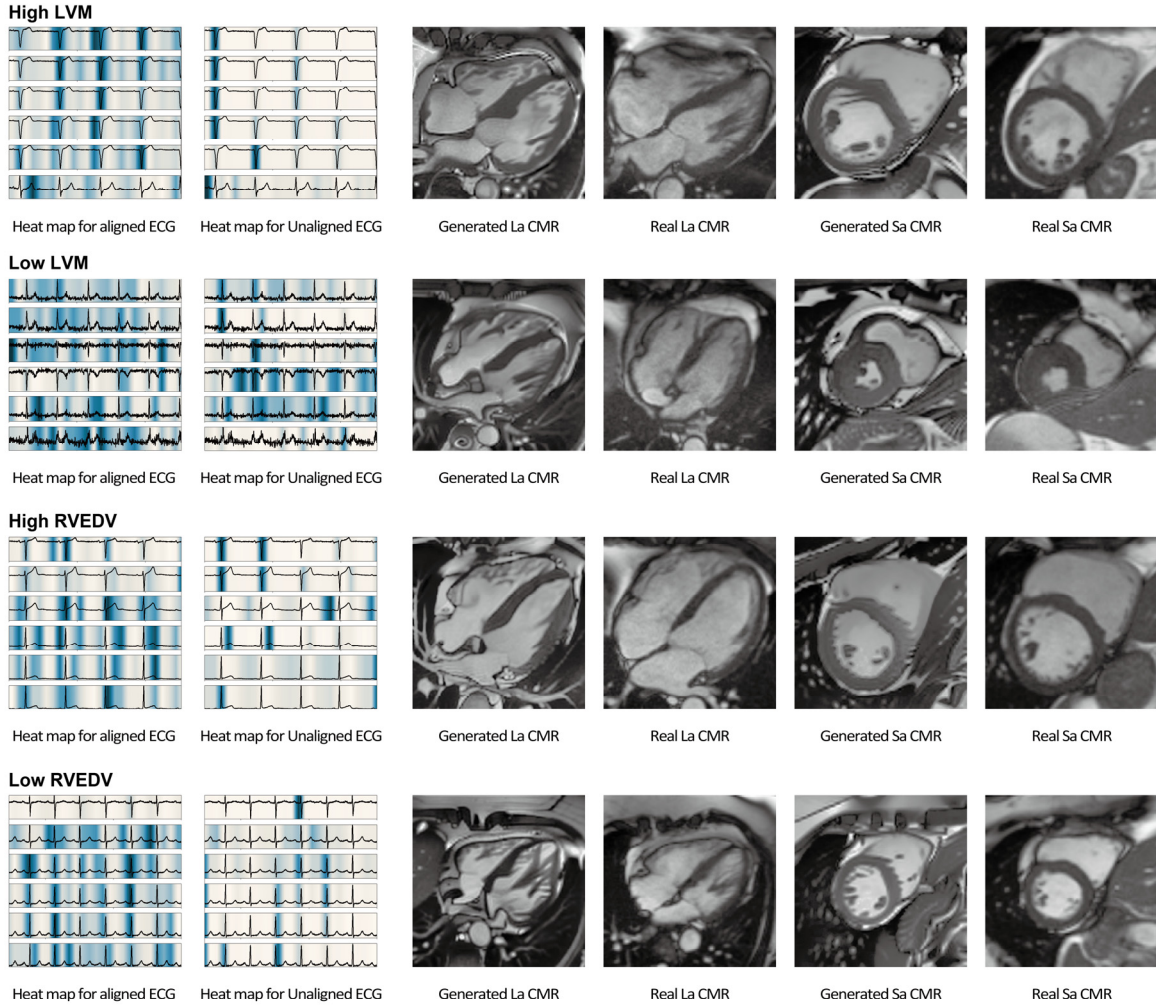
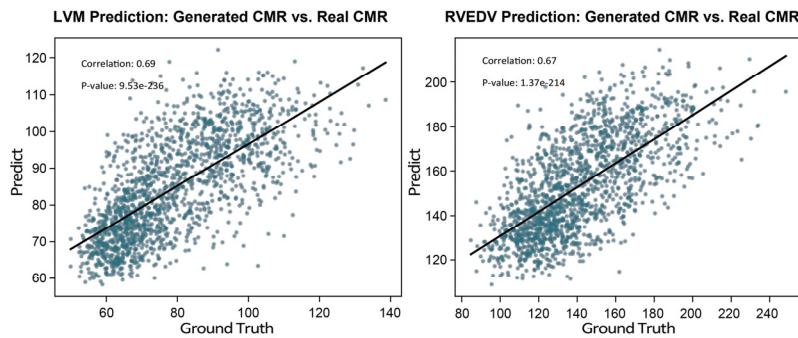


Fig. 3: Classification results of the three subtypes of cardiomyopathy. a. MIMIC dataset; b. FAHZU dataset.

a. Heatmap of ECG and comparison with real and generated CMR



b. Correlation analysis



c. Comparison with SOTA method

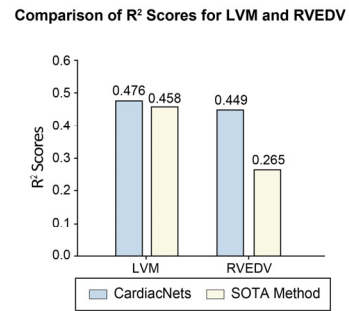


Fig. 4: Quality assessment of generated CMR images and Interpretability heatmap of ECG. **a.** The ECG-conditioned CMR diffusion model enables the generation of long and short axis CMR images from ECGs while accurately capturing MRI-specific features such as left ventricular mass (LVM) and right ventricular end-diastolic volume (RVEDV) on test MRI-ECG pairs. Examples qualitatively demonstrate that MRIs imputed from test ECG samples reflect LVM and RVEDV for individuals in the highest and lowest deciles. **b.** The correlation between the phenotypes predicted by the generated CMRs. **c.** Comparison with the model proposed by Radhakrishnan et al.,²³ for LVM and RVEDV estimation.

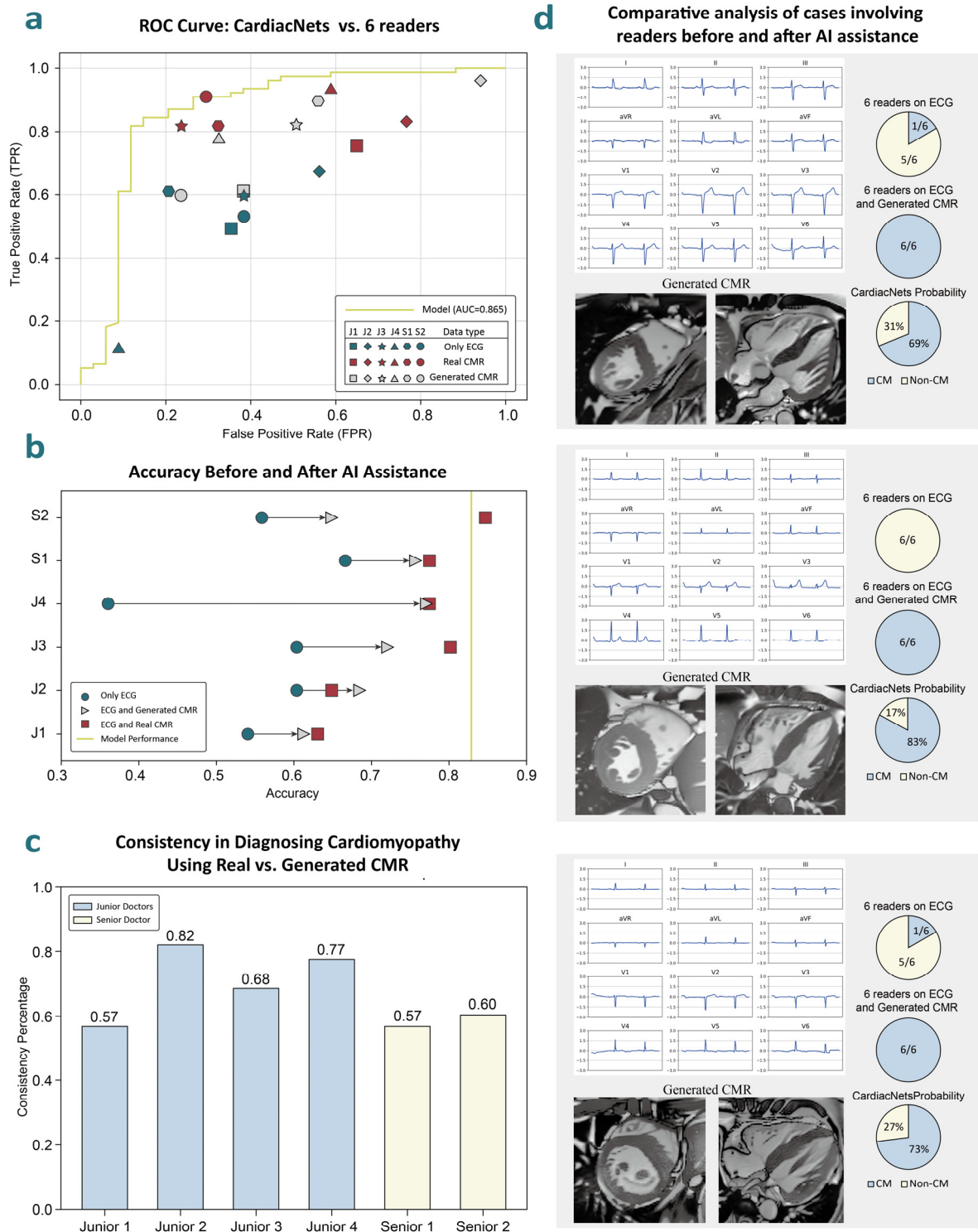


Fig. 5: Reader study. **a.** Performance of AI models and physicians in detecting cardiomyopathy across two stages: the first stage involved screening based solely on ECG interpretation, while the second stage provided physicians with either AI-generated or real CMR images. **b.** Improvement in physicians' accuracy when assisted by AI-generated data. **c.** Consistency analysis of physicians' diagnoses when observing real CMR images versus AI-generated CMR images for the same patients. **d.** Three cases where cardiomyopathy was initially missed when relying only on ECG, but correctly identified with the assistance of AI.

Discussion

In this study, we propose CardiacNets, a cross-modal pretraining model that employs a pretraining-finetuning paradigm to efficiently adapt to the screening of a broad spectrum of CVDs. Additionally, the visualizations generated by the model bolster the interpretability of the results. CardiacNets demonstrates substantial potential for utilizing ECG in the screening of cardiovascular diseases, particularly in economically underdeveloped regions where access to advanced diagnostic tools may be limited.

Building on previous work²⁴, we acknowledge that while focusing on a specific task and obtaining CMR model weights through supervised learning can enhance the ECG model's performance using contrastive loss training, this approach has a significant limitation: it does not leverage the inherent paired information between ECG and CMR. As a result, each time a new task arises, we must retrain both the CMR supervised model and the ECG alignment model specifically for that task. To address this limitation, we developed a model that introduces a critical shift from prior approaches: we utilize a self-supervised²⁷ method to comprehensively learn the structural information of CMR. This encapsulates a holistic representation of cardiac status that serves as a foundation for analyzing downstream tasks. In our self-supervised pretraining model, we freeze the parameters of the CMR model and update the ECG model by minimizing contrastive loss. This allows the ECG model to extract essential features that represent the overall cardiac state inherent to CMR, independent of specific tasks. These features exhibit strong discriminative capabilities across various downstream tasks. For CMR, we implement a masked self-supervised learning approach²⁸ using the GreenMIM²⁹ framework based on the Swin Transformer³⁰. Unlike conventional Vision Transformers (ViTs)³¹, the unique shifted window mechanism of the Swin Transformer creates a receptive field akin to that of Convolutional Neural Networks (CNNs)³², effectively addressing the limitations of ViTs in capturing local details in images³³—an essential aspect of medical image analysis. For ECG, which is inherently a periodic time-series signal, we employ a modified ViT for encoding. This enables attention computation across independent blocks, allowing for a more comprehensive focus on information compared to traditional time-series models such as Recurrent Neural Networks (RNNs)³⁴.

The results of CardiacNets on the UKB and MIMIC datasets demonstrate that the model significantly enhances the performance of ECG, particularly in smaller datasets, approaching the upper limits achieved through supervised learning with CMR. In contrast, this improvement is less pronounced in larger datasets, which is understandable: deep learning methods rely on large sample sizes to accurately approximate true distributions; therefore, the more data available, the better the model's fitting capacity³⁵. However, even within the MIMIC dataset, where the number of samples for CAD and HF exceeds two to three hundred thousand, models trained using ECG-CMR paired learning consistently outperform those based solely on supervised learning with ECG. This observation indicates that there is an upper limit to what can be achieved with ECG alone, primarily due to the lack of cross-modal structural information that CMR provides. This underscores the effectiveness of our cross-modal solution.

Interpretability is essential in clinical settings³⁶, and CardiacNets introduces an innovative video diffusion model conditioned on ECG to generate temporal CMR images. This approach allows for the creation of CMR images even in the absence of actual CMR data, serving as a valuable tool for both explainability and visualization. While existing video diffusion models, such as Sora³⁷, have made significant advances in areas like artistic creation, their use in medical imaging is still limited. This

limitation arises from two main factors: first, the differing domain requirements: medicine prioritizes evidence-based practices³⁸ over creativity, which contrasts with the objectives of mainstream video diffusion models. Second, medical datasets often consist of only hundreds or thousands of samples³⁹, making it difficult to fully harness the potential of these models. Specifically, we leverage the diffusion model within CardiacNets as an interpretable tool that provides physicians with enhanced explainability and visualization. By utilizing the aligned ECG encoder as a precise guide and fine-tuning the video diffusion model with a large-scale cross-modal dataset of approximately 40,000 samples, we achieve the generation of high-resolution, high-fidelity CMR images. Moreover, these images can effectively capture specific cardiac structural information (Fig. 4 and Fig. 5).

There is substantial evidence indicating that the most commonly used screening tests for cardiovascular disease—ECG and echocardiography—capture only a limited amount of the diagnostic information necessary for effective CVD anomaly detection^{40,41}. In contrast, CMR is regarded a common and effective diagnostic tool for CVDs⁴². However, CMR presents significant challenges in large-scale disease screening due to the complexities of cardiac motion, intricate operational procedures, and high examination costs¹⁸. This naturally raises the question of whether ECG, which is simpler and more accessible, could be used as a substitute for CMR in CVD screening. The introduction of CardiacNets demonstrates high performance across a range of downstream tasks, which shows that the model can extract and represent comprehensive cardiac information, including certain structural features, from CMR using only ECG data. It allows individuals to assess their cardiovascular health and disease risk through routine examinations in simplified community hospital settings, ultimately reducing the risks associated with delayed treatment. Of note, we observed high specificity scores of 83.5%, 99.5%, and 99.1% across three private external validation datasets for cardiomyopathies. This underscores the model's potential as a large-scale opportunistic screening tool, which could further alleviate the significant burden CVD places on healthcare systems and society.

In the reader study, CardiacNets, utilizing only ECG input, performed comparably to senior physicians evaluating both ECG and CMR, while significantly outperforming those who relied solely on ECG data. With the assistance of CMR generated by the model, all physicians' performance showed substantial improvement compared to when they used only ECG, underscoring the model's potential for real-world screening and clinical decision support. Notably, physicians demonstrated higher sensitivity with actual CMR images compared to model-generated outputs, reflecting a clinical diagnostic logic that effectively mitigates Type II errors (Supplementary Table 9). While our model achieves a favourable balance between specificity and sensitivity, as indicated by a high AUC, it is necessary to integrate the diagnostic logic of physicians into the model learning for enhancing human-machine interaction and fusion, potentially boosting the model's interpretability and clinical utility.

Our study demonstrates that ECG can not only be used to screen for cardiomyopathy but also effectively identify its three subtypes. Cardiomyopathy is typically regarded as an irreversible heart disease⁴³, and distinct subtypes exhibit significant differences in cardiac structure and morphology⁴³. These differences necessitate distinct treatment and prognostic approaches tailored to each subtype⁴⁴. Therefore, early screening of cardiomyopathy subtypes is essential to support precision medicine and slow disease progression. In clinical diagnosis, precise identification of cardiomyopathy subtypes typically requires a comprehensive diagnostic workflow: the initial step usually involves CMR screening to categorize subtypes⁴⁵, followed by a second step involving myocardial biopsy or genetic test⁴⁶ for biomarker

extraction to confirm the diagnosis. Given the complexity of cardiomyopathy, the diagnostic process for its subtypes resembles a branching structure rather than a linear pathway⁴⁷, making CMR-based screening indispensable as a first step. The proposed solution can provide early probabilistic classification of cardiomyopathy subtypes using ECG alone (Fig. 3). This finding highlights the potential for our model to replace CMR in subtype diagnosis, thereby streamlining the diagnostic process and conserving medical resources.

Several limitations must be considered when interpreting the results presented. Firstly, although we have validated the effectiveness of our solution using extensive datasets from the UK, USA, and China, it is important to acknowledge that our pretrained model is based entirely on approximately 40,000 ECG-CMR paired samples from the UK Biobank. The UK Biobank is known to contain racial and socioeconomic biases, which can result in significant inequities in healthcare⁴⁸. Therefore, it is essential to retrain or update our model using a more diverse population and to conduct a thorough analysis of how well our model generalizes to underrepresented cohorts before applying this method in clinical settings. Secondly, further research is needed to address the interpretability of deep learning models. While the Grad-CAM results in Fig. 4 demonstrate explainability for downstream tasks based on ECG predictions, the interpretability of how the ECG guides the diffusion model to generate CMR images requires further exploration. Finally, extensive evaluation through prospective studies and clinical trials is necessary before clinical implementation of our models. The algorithmic performance reported in this study may not directly translate to real-world clinical scenarios, underscoring the need for additional validation.

In conclusion, this work validates a cross-modal learning approach for cardiac function assessment using only ECG, paving the way to enhance CVD screening and diagnosis at the population level. Furthermore, the successful application of our model in the ECG-CMR domain highlights its potential for analyzing other paired datasets with strong-weak modality relationships, opening new avenues for multimodal research across diverse medical contexts.

Methods

Dataset for Model Development and Evaluation

We utilized the UK Biobank¹⁹, the largest publicly available dataset containing paired ECG and cine CMR imaging data, to advance our study. The UKB encompasses a diverse cohort of 500,000 volunteers aged 40 to 69, recruited across the UK since 2006, with ongoing data collection efforts. For our study, we focused on ECG-CMR pairs collected during participants' initial imaging visits, yielding a total of 41,519 paired datasets. The ECG data comprises 12-lead recordings, each lasting 10 seconds and sampled at 500 Hz, while the cine CMR data includes both short-axis and four-chamber long-axis views, each capturing a single cardiac cycle with 50 frames. The dataset exhibits a gender distribution of 48.3% male and 51.7% female participants. In terms of ethnicity, the majority of participants are White (96.6%), with smaller representations of Mixed (0.5%), Asian or Asian British (1.1%), Black or Black British (0.7%), Chinese (0.3%), and other ethnic groups (0.5%). Additionally, 0.3% of participants preferred not to disclose their ethnicity or were uncertain. The ethnicity classifications adhere to the UKB Data-Coding system (1001). Leveraging the UKB data, we developed our Contrastive ECG-CMR Pre-training model and the ECG2CMR Diffusion Model. The dataset was divided into training, validation, and test sets using a 7:1:2 ratio, ensuring a robust solution for model evaluation and development.

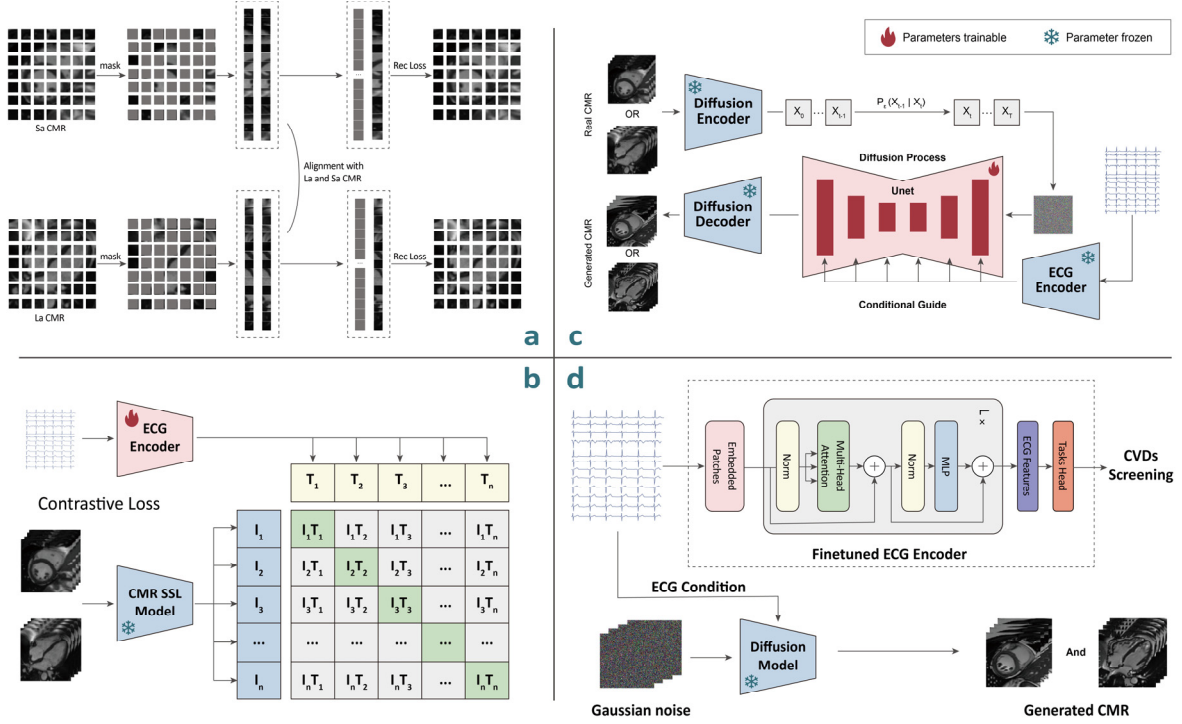


Fig. 6: Model diagram. **a.** CMR self-supervised model, leveraging the GreenMIM framework for masked self-supervised learning, optimized to minimize reconstruction loss and contrastive loss between long axis and short axis CMR images. **b.** ECG-CMR contrastive learning, with the parameters of the CMR self-supervised model in **subgraph a** frozen, optimized to minimize contrastive loss. **c.** ECG-guided CMR image generation, using the pre-trained ECG encoder in **subgraph b** as the conditional encoder for the diffusion model. The diffusion model's autoencoder and ECG encoder are frozen, and only the U-Net component is trained. **d.** Fine-tuning the aligned ECG encoder to adapt to various downstream tasks and use pretrained diffusion model in **subgraph c** generate the corresponding CMR images.

For our downstream analyses, we utilized the UKB and the MIMIC-IV-ECG⁴⁹ datasets, alongside private datasets from three hospitals: the First Affiliated Hospital of Zhejiang University School of Medicine (FAHZU), the Second Affiliated Hospital of Zhejiang University School of Medicine (SAHZU), and Quzhou People's Hospital (QPH). We selected 305,419 CVD samples and 195,753 non-CVD samples as controls from the MIMIC-IV-ECG dataset. In the UKB dataset, 3,822 CVD individuals and 3,822 non-CVD controls were chosen. Notably, the dataset splits used for downstream tasks in UKB were derived from pretraining splits to ensure no data leakage. The ECG data formats in both MIMIC and UKB datasets are consistent, recorded at 500 Hz for 10 seconds. In these public datasets, our focus was on classifying several cardiovascular conditions, including coronary artery disease (CAD, ICD-10 codes I20-I25), pulmonary hypertension (I27), pericarditis (I30-I32), cardiomyopathy (I42-I43), and heart failure (I50). To maintain a balanced positive-to-negative ratio across the datasets, we employed a methodology that involved selecting an equal number of negative cases for comparison, as suggested by prior studies⁵⁰. Additionally, we aimed to predict 82 cardiac structural indicators, as outlined in Supplementary Table 6. All conditions were classified according to the International Classification of Diseases, Tenth Revision (ICD-10). It is noteworthy that cases of pulmonary hypertension were infrequent in the UKB and were therefore excluded from our analysis. Note that the MIMIC-IV-ECG lacks corresponding CMR images, rendering the assessment of cardiac structural indicators impossible.

The FAHZU dataset is divided into three distinct subsets: the first subset includes only ECG data for a three-class classification of cardiomyopathy, encompassing 5,518 cases of dilated cardiomyopathy, 2,546 cases of hypertrophic cardiomyopathy, and 824 cases of restrictive cardiomyopathy. The second subset, also based solely on ECG data, is intended for external validation of cardiomyopathy, comprising 222 patients diagnosed with cardiomyopathy and 188 individuals without the condition. The third subset consists of ECG-CMR paired data for a reader study, including 77 patients with cardiomyopathy and 34 individuals without the condition. The SAHZU dataset includes 264 patients diagnosed with cardiomyopathy and 200 individuals without the condition, while the QPH dataset contains 236 cardiomyopathy patients and 102 non-cardiomyopathy individuals. Both of these private datasets are employed for external validation of cardiomyopathy. Importantly, all datasets utilized ECG formats consistent with that of the UKB dataset. Detailed data distributions for all datasets are provided in Supplementary Table 7. Except for the datasets designated for external validation, all remaining datasets were partitioned into training, validation, and testing sets in a 70:10:20 ratio.

Data processing and augmentation

We implemented a series of signal pre-processing techniques on all collected ECG data to enhance the quality and reliability of the signals for subsequent analysis. Initially, baseline drift was addressed using seasonal decomposition, allowing us to isolate and correct the trend component effectively. Following this, we applied wavelet transform denoising using the “db6” wavelet along with soft thresholding. This approach effectively reduced noise while preserving critical signal characteristics, ensuring that the integrity of the ECG waveform was maintained. Finally, we employed a Savitzky-Golay filter⁵¹ to smooth the signal. This filter utilizes polynomial fitting within a sliding window to refine the ECG waveform further. Collectively, these pre-processing steps ensured the generation of clean and reliable data, facilitating robust analysis in our study.

The original data for short-axis cardiac magnetic resonance (CMR) images is structured in four dimensions: length, width, slice, and time. Typically, the slice dimension comprises 3 to 10 slices. To streamline the model input, we selected the middle basoapical slice, reformulating the data into a three-dimensional structure, where the time dimension consists of 50 frames. To focus the model on the cardiac region, we employed a pretrained segmentation model⁵² to derive a heart region mask. The images were then cropped to 80×80 pixels, centering on the minimal bounding box encompassing the non-zero region of the mask. For long-axis four-chamber CMR images, the original data is three-dimensional, consisting of length, width, and time dimensions, with the time dimension also comprising 50 frames. Using the same segmentation methodology applied to the short-axis images, we cropped the long-axis images to 96×96 pixels. This adjustment was necessary due to the larger heart region captured in this view, ensuring that the entire heart was included within the cropped area.

In the Contrastive ECG-CMR pre-training and downstream tasks, we employed several data augmentation techniques. For the ECG data, we implemented crop resizing, time reversal (TimeFlip), and sign inversion (SignFlip). These transformations were followed by Min-Max scaling within a range of -1 to 1 on a channel-wise basis. During validation and testing, only Min-Max scaling was applied. For the CMR data, we utilized random rotation (up to 30 degrees), random horizontal and vertical flips, and random resized cropping with a scale range of 0.8 to 1.0 and an aspect ratio of 0.9 to 1.1. This was succeeded by resizing the images to 256×256 pixels using bilinear interpolation. Normalization was applied across all 50 frames of both short-axis and long-axis images, using a mean of 0.5 and a standard

deviation of 0.5. During validation and testing, only normalization and resizing were performed to ensure consistency in the evaluation process.

During the training phase of the diffusion model, we focused on preserving critical data features, including the waveform characteristics of the ECG and the orientation of the heart in the CMR images. As such, we applied only Min-Max scaling to the ECG data and resizing to the CMR images.

Self-supervised method for CMR

We initially employed self-supervised learning on the CMR images to obtain robust representations for subsequent Contrastive ECG-CMR pre-training, as shown in Fig. 6a. The Swin Transformer base served as the backbone, utilizing GreenMIM²⁹ for masked self-supervised training. The encoder patch size was set to 4×4 , with a window size of 7. For both long-axis and short-axis CMR images, the temporal dimension (50 frames) was treated as the number of channels in the 2D images, with masking applied separately to each channel. In addition to the reconstruction loss aimed at restoring the original images, we introduced contrastive learning losses post-encoder for both long-axis and short-axis images to align and enhance the information between the two. Qualitative results can be found in Extended Fig. 2. The masking ratio was set to 0.75 during model training on an 80GB A800 GPU, utilizing a batch size of 32 over 400 training epochs. The first 40 epochs focused on learning rate warm-up, gradually increasing the learning rate from 0 to 1×10^{-4} . The final model weights were saved as checkpoints for downstream tasks.

Contrastive ECG-CMR Pre-training

We employed a ViT-Large³¹ model as the ECG encoder and utilized a frozen, self-supervised Swin Transformer as the CMR encoder, as shown in Fig. 6b. The ECG encoder processes data in the format [b, 12, 5000], where 12 corresponds to the 12 ECG leads, and 5000 represents 10 seconds of data at 500 Hz. This data is treated as a 1-channel image with dimensions 12×5000 , and we applied a ViT model with a patch size of (1,100), resulting in 600 patches. Standard ViT processing is subsequently applied to these patches. For the CMR model, we utilize the encoder from the aforementioned self-supervised model, while keeping its parameters frozen. During training, the features encoded from the ECG are compared with those from both long-axis and short-axis CMR images in a contrastive learning setup, with the total loss being the sum of these two comparisons. The model was trained on an 80G A800 GPU with a batch size of 8, with the first 40 epochs dedicated to learning rate warm-up (from 0 to 1×10^{-4}). The model checkpoint with the lowest validation loss was saved for downstream tasks.

ECG2CMR Diffusion Model

We adapted the architecture of a text-to-video model²⁶ to develop our ECG2CMR model, as shown in Fig. 6c. It's a latent diffusion model comprising three main components. The first component is an autoencoder that transforms CMR data into a low-dimensional latent space and subsequently decodes it back to pixel space. For this purpose, we utilized a pretrained model on natural images, keeping its parameters frozen. The second component is a denoising U-Net, which exhibits slight variations from the standard U-Net used in text-to-image models. It comprises four key structures: the initial block, down-sampling blocks, spatiotemporal blocks, and up-sampling blocks. The initial block projects the input into the embedding space, while the down-sampling and up-sampling blocks adjust the spatial resolution of the feature maps. The spatiotemporal block is crucial for capturing complex spatial and temporal dependencies in the latent space, thereby enhancing the quality of the synthesized CMR images.

This U-Net was initialized using pre-trained weights from a text-to-video diffusion model. The third component, which distinguishes our approach from typical text-to-video models, is the conditional encoder. We employed the frozen ECG encoder from the previously pre-trained ECG model as the conditional encoder, utilizing cross-attention to guide the training of the diffusion model. Due to the significant differences between long-axis and short-axis CMR images, we trained two separate models to generate each type of CMR image.

In the forward process of diffusion model training, when a CMR image $x_0 \sim p(x)$ is input, it first passes through the latent encoder \mathcal{E} , and gets the latent features $z_0 = \mathcal{E}(x_0)$. Assuming $z_0 \sim q(z)$, the diffusion process adds Gaussian noise incrementally over T timesteps, yielding latent vectors z_0, z_1, \dots, z_T , governed by the following distributions:

$$q(z_t | z_{t-1}) = \mathcal{N}(z_t; \sqrt{1 - \beta_t} z_{t-1}, \beta_t \mathbf{I}) \quad (1)$$

$$q(z_t | z_0) = \mathcal{N}(z_t; \sqrt{\bar{\alpha}_t} z_0, (1 - \bar{\alpha}_t) \mathbf{I}) \quad (2)$$

where $\alpha_t = 1 - \beta_t$, $\bar{\alpha}_t = \prod_{i=1}^t \alpha_i$, and β_t is the noise schedule, linearly increasing from 0.0001 to 0.02. As $t \rightarrow \infty$, z_t approaches pure Gaussian noise. The reverse process aims to recover z_0 from z_T . Using Bayes' rule, the reverse distribution is:

$$q(z_{t-1} | z_t, z_0) = \mathcal{N}(z_{t-1}; \tilde{\mu}(z_t, z_0), \tilde{\beta}_t \mathbf{I}) \quad (3)$$

where $\tilde{\mu}(z_t, z_0)$ is predicted by the neural network $U_\theta(z_t, t, c)$, and c represents the conditional features from the ECG conditional encoder. Finally, the latent vector \tilde{z}_0 is decoded back to pixel space \tilde{x}_0 via the latent decoder. The training objective is:

$$L_{LDM} = E_{\mathcal{E}(x), y, \epsilon \sim \mathcal{N}(\mathbf{0}, \mathbf{I}), t} [|\epsilon - \epsilon_\theta(z_t, t, \tau_\theta(y))|_2^2] \quad (4)$$

where x is the CMR images, y is the ECG signal, \mathcal{E} is the latent encoder, and ϵ_θ is the noise predicted by the Unet. The training was conducted on a single 80G A800 GPU, with a batch size of 4 and a learning rate maintained at 3e-6. After each epoch, the model was evaluated on the validation set, and the weights corresponding to the lowest loss were saved as model checkpoints for CMR generation. During inference, CMR images were generated by sampling from Gaussian noise and iteratively denoising under the guidance of the ECG, utilizing the DDIM sampling method⁵³, which required around 100 steps to produce a single image.

Downstream tasks

In adapting to downstream tasks, we utilized only the ECG encoder from the Contrastive ECG-CMR Pre-training model, excluding the CMR encoder, as shown in Fig. 6d. The ECG encoder generates high-level features from ECG signals that embed CMR information. Additionally, we incorporated demographic and lifestyle factors specific to each dataset through feature modulation for joint training. For the UKB dataset, these factors included age at assessment center visit, frequency of alcohol intake, body mass index (BMI), days per week engaging in moderate-intensity physical activity lasting at least 10 minutes, sex, sleep duration, smoking status, standing height, stress levels/high stress, weight, intake of raw vegetables, days per week walking at least 10 minutes, pork intake, insomnia, and average heart

rate. For other datasets, the factors used were sex, age, and average heart rate. For binary classification tasks, we followed the methodology outlined in reference⁵⁰, maintaining a balanced ratio of approximately 1:1 for positive and negative samples. For the CMR generation model, we employed the pre-trained diffusion model (Fig. 6c) to generate high-fidelity CMR images containing authentic cardiac information, offering clinicians valuable visual and interpretive insights.

In our experiments, we fine-tuned the entire ECG encoder to accommodate the varying data distributions of each task, except for the external validation datasets where the trained model was directly used for inference. The training objective was to generate classification outputs that aligned with CVD labels or regression outputs that closely approximated the ground truth values of 82 cardiac structural indicators. We set the batch size to 10 and allowed for a maximum of 400 training epochs. To prevent unnecessary training, we employed early stopping, dedicating the first 10 epochs to a learning rate warm-up from 0 to 1×10^{-4} , followed by cosine annealing to 0. After each epoch, the model was evaluated on the validation set, and the weights corresponding to the highest AUROC on the validation set were saved as checkpoints for internal evaluation across datasets.

Quantitative assessment and statistical analysis

For classification tasks, we employed several evaluation metrics: area under the curve (AUC), accuracy, sensitivity, specificity, positive predictive value (PPV), and negative predictive value (NPV). In our three-class classification, we binarized the labels using a one-vs-rest approach prior to evaluation. For regression tasks related to cardiac indices, we used the Pearson correlation coefficient as the primary metric. To compute 95% confidence intervals, we applied the Wilson Score Interval⁵⁴ for classification metrics and the bootstrap method⁵⁵ for regression metrics. For method comparisons, we utilized the DeLong test for AUC, while other metrics were assessed using two-sided z-tests.

Software for data process and model development

We utilized several libraries for data processing and model development, including numpy (version 1.25.2)⁵⁶, sklearn (version 1.1.1)⁵⁷, scipy (version 1.11.2)⁵⁸, simpleITK (version 2.3.1)⁵⁹ and pandas (version 2.2.1). For model development, we employed pytorch (version 1.11.0).

Competing Interests

The authors declare no competing interests.

Acknowledgements

The authors thank all study participants and staff for contributing to the UK Biobank Cohort under application number 89757.

Data availability

The data used in the study that supports cross-modal pre-training were obtained from the UK Biobank under application number 89757. Access to the UK Biobank data is available to all researchers with approval (<https://www.ukbiobank.ac.uk/enable-your-research/register>). The data used in the study that supports downstream tasks were obtained from the MIMIC-IV-ECG database, accessible via PhysioNet under credentialed access (<https://physionet.org/content/mimic-iv-ecg/1.0/>).

For the data from three private hospitals, the requirement for informed consent was waived by the respective ethics committees and institutions. The de-identified data can be shared only for non-

commercial academic purposes and will require a formal material transfer agreement and a data use agreement. Requests should be submitted by emailing the corresponding authors (ZH, HZ, or TC) at zhengxinghuang@zju.edu.cn, doczhk@163.com, or ct010151452@zju.edu.cn. All requests will be evaluated based on institutional policies to determine whether the requested data are subject to intellectual property or patient privacy obligations. Generally, all such requests for access to data will be responded to within 1 month.

Code availability

The source codes about this study and data analysis in this manuscript are provided at <https://github.com/Yukui-1999/ECG-CMR>.

Author contributions

ZH, HZ and FW jointly supervised research. ZH designed this study. ZD and YH developed a deep learning model and performed the model interpretation. ZD, ZY Li, YM and HL performed data analysis. ZD, YH, WP, ZY Liu, XC, FW, TC, HZ and ZH interpreted the results. TC, QL, JW, YC, MC, LW, YX and CZ participated in the reader study. ZD, YH, TC and ZH prepared the first draft of the manuscript. All authors contributed and approved the final draft.

Extended Fig

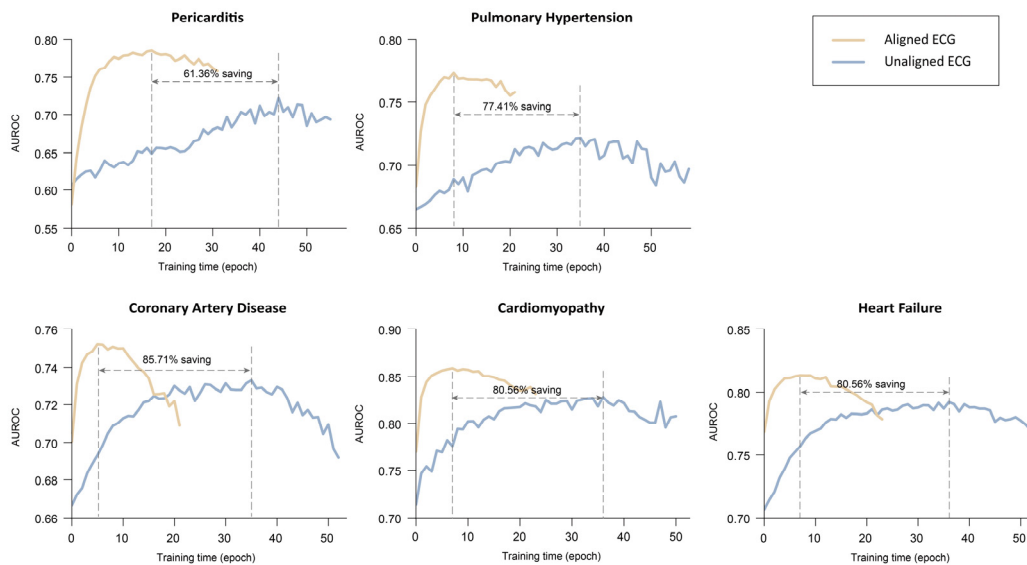


Fig. 1: Adaptation Efficiency. Time required to reach convergence epoch for fine-tuning a pretrained model versus training a supervised model directly in the MIMIC dataset

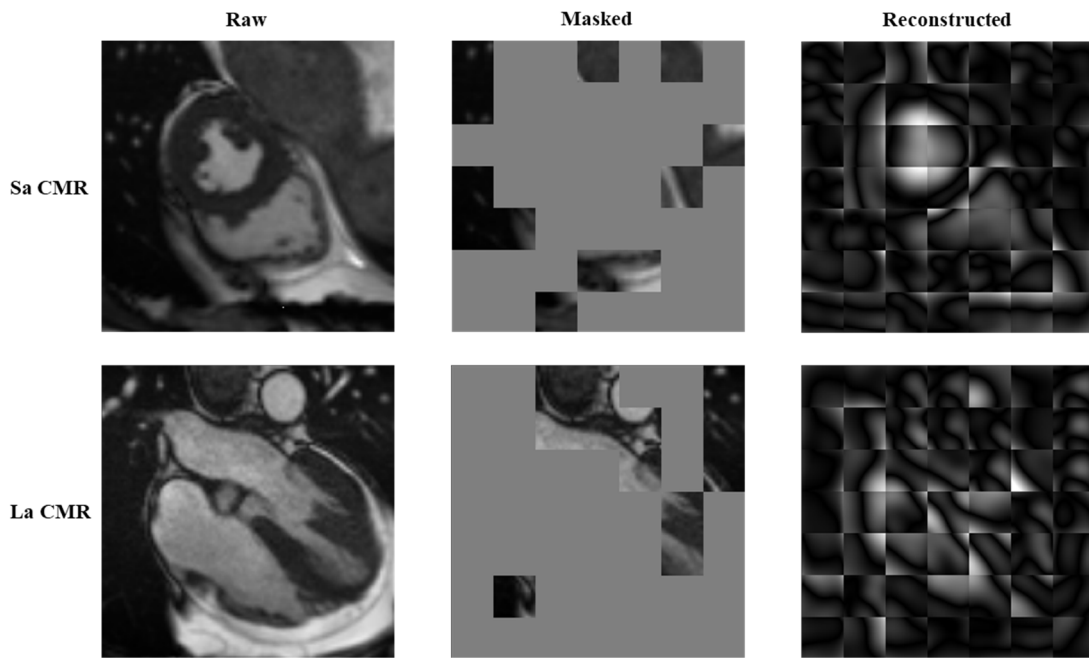


Fig. 2: CMR self-supervised. Result of CMR self-supervised learning using the GreenMIM framework. This approach enables learning of essential information from $\hat{\text{CMR}}$ images for use during ECG alignment. Sa CMR, short axis cine CMR images; La CMR, long axis cine CMR images.

References

1. Zhao, D. Epidemiological Features of Cardiovascular Disease in Asia. *JACC Asia* **1**, 1-13 (2021).
2. Timmis, A., *et al.* European Society of Cardiology: cardiovascular disease statistics 2021. *Eur Heart J* **43**, 716-799 (2022).
3. Tsao, C.W., *et al.* Heart Disease and Stroke Statistics-2023 Update: A Report From the American Heart Association. *Circulation* **147**, e93-e621 (2023).
4. Mortality, G.B.D. & Causes of Death, C. Global, regional, and national life expectancy, all-cause mortality, and cause-specific mortality for 249 causes of death, 1980-2015: a systematic analysis for the Global Burden of Disease Study 2015. *Lancet* **388**, 1459-1544 (2016).
5. Cheng, S., Han, Y., Jiang, L., Lan, Z. & Guo, J. National, regional, and global cardiomyopathy burden from 1990 to 2019. *Front Cardiovasc Med* **9**, 1042448 (2022).
6. Roth, G.A., *et al.* Global, Regional, and National Burden of Cardiovascular Diseases for 10 Causes, 1990 to 2015. *J Am Coll Cardiol* **70**, 1-25 (2017).
7. De Bacquer, D., De Backer, G., Kornitzer, M. & Blackburn, H. Prognostic value of ECG findings for total, cardiovascular disease, and coronary heart disease death in men and women. *Heart* **80**, 570-577 (1998).
8. Arnold, J.R. & McCann, G.P. Cardiovascular magnetic resonance: applications and practical considerations for the general cardiologist. *Heart* **106**, 174-181 (2020).
9. Rawi, A.A., Albashir, M.K. & Ahmed, A.M. Classification and detection of ECG arrhythmia and myocardial infarction using deep learning: a review. *Webology* **19**, 1151-1170 (2022).
10. Salerno, M. & Kramer, C.M. Advances in parametric mapping with CMR imaging. *JACC Cardiovasc Imaging* **6**, 806-822 (2013).
11. Jerosch-Herold, M. Quantification of myocardial perfusion by cardiovascular magnetic resonance. *J Cardiovasc Magn Reson* **12**, 57 (2010).
12. Friedrich, M.G. Tissue characterization of acute myocardial infarction and myocarditis by cardiac magnetic resonance. *JACC Cardiovasc Imaging* **1**, 652-662 (2008).
13. Rajiah, P.S., Francois, C.J. & Leiner, T. Cardiac MRI: State of the Art. *Radiology* **307**, e223008 (2023).
14. Wang, Y.-R., *et al.* Screening and diagnosis of cardiovascular disease using artificial intelligence-enabled cardiac magnetic resonance imaging. *Nature Medicine*, 1-10 (2024).
15. Ibrahim, E.H., *et al.* Value CMR: Towards a Comprehensive, Rapid, Cost-Effective Cardiovascular Magnetic Resonance Imaging. *Int J Biomed Imaging* **2021**, 8851958 (2021).
16. La Gerche, A., *et al.* Cardiac MRI: a new gold standard for ventricular volume quantification during high-intensity exercise. *Circ Cardiovasc Imaging* **6**, 329-338 (2013).
17. Salerno, M., *et al.* Recent Advances in Cardiovascular Magnetic Resonance: Techniques and Applications. *Circ Cardiovasc Imaging* **10**(2017).
18. Kim, R.J., *et al.* Guidelines for training in cardiovascular magnetic resonance (CMR). *J Cardiovasc Magn Reson* **20**, 57 (2018).
19. Sudlow, C., *et al.* UK biobank: an open access resource for identifying the causes of a wide range of complex diseases of middle and old age. *PLoS Med* **12**, e1001779 (2015).

20. Johnson, A.E.W., *et al.* MIMIC-IV, a freely accessible electronic health record dataset. *Sci Data* **10**, 1 (2023).
21. Radford, A., *et al.* Learning transferable visual models from natural language supervision. in *International conference on machine learning* 8748-8763 (PMLR, 2021).
22. Rombach, R., Blattmann, A., Lorenz, D., Esser, P. & Ommer, B. High-resolution image synthesis with latent diffusion models. in *Proceedings of the IEEE/CVF conference on computer vision and pattern recognition* 10684-10695 (2022).
23. Radhakrishnan, A., *et al.* Cross-modal autoencoder framework learns holistic representations of cardiovascular state. *Nat Commun* **14**, 2436 (2023).
24. Ding, Z., *et al.* Cross-Modality Cardiac Insight Transfer: A Contrastive Learning Approach to Enrich ECG with CMR Features. in *International Conference on Medical Image Computing and Computer-Assisted Intervention* 109-119 (Springer, 2024).
25. Turgut, Ö., *et al.* Unlocking the diagnostic potential of ecg through knowledge transfer from cardiac mri. *arXiv preprint arXiv:2308.05764* (2023).
26. Wang, J., *et al.* Modelscope text-to-video technical report. *arXiv preprint arXiv:2308.06571* (2023).
27. Krishnan, R., Rajpurkar, P. & Topol, E.J. Self-supervised learning in medicine and healthcare. *Nature Biomedical Engineering* **6**, 1346-1352 (2022).
28. He, K., *et al.* Masked autoencoders are scalable vision learners. in *Proceedings of the IEEE/CVF conference on computer vision and pattern recognition* 16000-16009 (2022).
29. Huang, L., *et al.* Green hierarchical vision transformer for masked image modeling. *Advances in Neural Information Processing Systems* **35**, 19997-20010 (2022).
30. Liu, Z., *et al.* Swin transformer: Hierarchical vision transformer using shifted windows. in *Proceedings of the IEEE/CVF international conference on computer vision* 10012-10022 (2021).
31. Dosovitskiy, A. An image is worth 16x16 words: Transformers for image recognition at scale. *arXiv preprint arXiv:2010.11929* (2020).
32. Indolia, S., Goswami, A.K., Mishra, S.P. & Asopa, P. Conceptual understanding of convolutional neural network-a deep learning approach. *Procedia computer science* **132**, 679-688 (2018).
33. Takahashi, S., *et al.* Comparison of Vision Transformers and Convolutional Neural Networks in Medical Image Analysis: A Systematic Review. *Journal of Medical Systems* **48**, 1-22 (2024).
34. Medsker, L.R. & Jain, L. Recurrent neural networks. *Design and Applications* **5**, 2 (2001).
35. Hestness, J., *et al.* Deep learning scaling is predictable, empirically. *arXiv preprint arXiv:1712.00409* (2017).
36. Tonekaboni, S., Joshi, S., McCradden, M.D. & Goldenberg, A. What clinicians want: contextualizing explainable machine learning for clinical end use. in *Machine learning for healthcare conference* 359-380 (PMLR, 2019).
37. Liu, Y., *et al.* Sora: A review on background, technology, limitations, and opportunities of large vision models. *arXiv preprint arXiv:2402.17177* (2024).
38. Sackett, D.L. & Rosenberg, W.M.C. On the need for evidence-based medicine. *Journal of Public Health* **17**, 330-334 (1995).
39. Schäfer, R., *et al.* Overcoming data scarcity in biomedical imaging with a foundational multi-task model. *Nature Computational Science* **4**, 495-509 (2024).

40. Valente, A.M., *et al.* Comparison of echocardiographic and cardiac magnetic resonance imaging in hypertrophic cardiomyopathy sarcomere mutation carriers without left ventricular hypertrophy. *Circulation: Cardiovascular Genetics* **6**, 230-237 (2013).
41. Capron, T., *et al.* Cardiac magnetic resonance assessment of left ventricular dilatation in chronic severe left-sided regurgitations: comparison with standard echocardiography. *Diagnostic and interventional imaging* **101**, 657-665 (2020).
42. Hundley, W.G., *et al.* ACCF/ACR/AHA/NASCI/SCMR 2010 expert consensus document on cardiovascular magnetic resonance: a report of the American College of Cardiology Foundation Task Force on Expert Consensus Documents. *Journal of the American College of Cardiology* **55**, 2614-2662 (2010).
43. Brieler, J., Breeden, M.A. & Tucker, J. Cardiomyopathy: an overview. *American family physician* **96**, 640-646 (2017).
44. Gimeno, J.R., *et al.* Prospective follow-up in various subtypes of cardiomyopathies: insights from the ESC EORP Cardiomyopathy Registry. *European Heart Journal-Quality of Care and Clinical Outcomes* **7**, 134-142 (2021).
45. Jan, M.F. & Tajik, A.J. Modern imaging techniques in cardiomyopathies. *Circulation research* **121**, 874-891 (2017).
46. McKenna, W.J., Maron, B.J. & Thiene, G. Classification, epidemiology, and global burden of cardiomyopathies. *Circulation research* **121**, 722-730 (2017).
47. Arbustini, E., *et al.* The MOGE (S) classification of cardiomyopathy for clinicians. *Journal of the American College of Cardiology* **64**, 304-318 (2014).
48. Obermeyer, Z., Powers, B., Vogeli, C. & Mullainathan, S. Dissecting racial bias in an algorithm used to manage the health of populations. *Science* **366**, 447-453 (2019).
49. Gow, B., *et al.* MIMIC-IV-ECG-Diagnostic Electrocardiogram Matched Subset. *Type: dataset* (2023).
50. Zhou, Y., *et al.* A foundation model for generalizable disease detection from retinal images. *Nature* **622**, 156-163 (2023).
51. Schafer, R.W. What is a savitzky-golay filter?[lecture notes]. *IEEE Signal processing magazine* **28**, 111-117 (2011).
52. Bai, W., *et al.* A population-based phenome-wide association study of cardiac and aortic structure and function. *Nature medicine* **26**, 1654-1662 (2020).
53. Song, J., Meng, C. & Ermon, S. Denoising diffusion implicit models. *arXiv preprint arXiv:2010.02502* (2020).
54. Wilson, E.B. Probable inference, the law of succession, and statistical inference. *Journal of the American Statistical Association* **22**, 209-212 (1927).
55. Tibshirani, R.J. & Efron, B. An introduction to the bootstrap. *Monographs on statistics and applied probability* **57**, 1-436 (1993).
56. Van Der Walt, S., Colbert, S.C. & Varoquaux, G. The NumPy array: a structure for efficient numerical computation. *Computing in science & engineering* **13**, 22-30 (2011).
57. Pedregosa, F., *et al.* Scikit-learn: Machine learning in Python. *the Journal of machine Learning research* **12**, 2825-2830 (2011).
58. Virtanen, P., *et al.* SciPy 1.0: fundamental algorithms for scientific computing in Python. *Nature methods* **17**, 261-272 (2020).
59. Lowekamp, B.C., Chen, D.T., Ibáñez, L. & Blezek, D. The design of SimpleITK. *Frontiers in neuroinformatics* **7**, 45 (2013).